# Time-Domain Imaging of Radar Targets Using Sinogram Restoration for Limited-View Reconstruction

Yingcheng Dai, E. J. Rothwell, *Senior Member, IEEE,* K. M. Chen, *Fellow, IEEE,* D. P. Nyquist, *Fellow, IEEE*

***Abstract*—The time-domain image reconstruction problem can be formulated as a sinogram recovery problem. The sinogram recovery problem is to find a complete sinogram based on the measured incomplete sinogram. In this paper, we solve the sinogram recovery problem by using linear prediction techniques. Since the scattered field of a target can be written as a superposition of distinct specular reflections arising from scattering centers on the target, the trace of the scattering centers can be predicted using linear prediction with the change of the observation angle. Thus, the missing data may be predicted before reconstructing the image. Some useful results obtained using the proposed method are presented.**

***Index Terms*—Radar imaging.**

## I. Introduction

THE development of viable short-pulse radar systems has sparked interest in target imaging performed directly in the time domain with temporally measured signals. The short-pulse response of a target provides significant information about the positions and strengths of scattering centers. If observations are made over a wide range of aspect angles, sufficient information is gained to obtain an image of the target. The authors have recently proposed a rigorous imaging identity based on a signal with spectral content limited to a portion of the electromagnetic (EM) spectrum. This makes it ideal for use with an ultrawide-band stepped frequency radar. However, as shown in [1] and [2], good images of radar targets may be obtained only when enough high quality data over a 180° angular range is available. When some data is missing, the reconstructed image suffers and may be unsatisfactory. In practice, information is usually available only for limited-view angles; thus, it is necessary to analyze the effect of incomplete information which may cause the inverse problem to be ill posed. The limited-view problem occurs when the data is available over an angular range less than 180° and the sparse-angle problem occurs when only a small number of angles evenly spaced over 180° are available.

The limited-view problems has attracted considerable attention in computed tomography imaging research and techniques for dealing with it have been proposed. These techniques can be put into two categories [12]: transform techniques that incorporate no *a priori* information and finite series expansion methods that may incorporate *a priori* information as constraints. The transform techniques are usually single-pass, direct reconstructions [3]–[5], while the finite series expansion methods are usually iterative [6]–[12].

Image reconstruction from incomplete projections can be formulated as a sinogram-recovery problem. The sinogram-recovery problem is to find a complete sinogram $A(t_s, \phi)$ based on the measured incomplete sinogram $A'(t_s, \phi)$ and *a priori* knowledge about the sinogram. Once an estimation of the complete sinogram is obtained, image reconstruction by ordinary convolution backprojection is possible.

In this paper, we will demonstrate a new reconstruction algorithm for radar imaging in the limited-angle case. The goal of this approach is to recover the sinogram from available measured data using linear prediction. Since the scattered field of a target can be written as a superposition of distinct specular reflections arising from scattering centers on the target, the trace of the scattering centers can be predicted using linear prediction with the change of the observation angle. Thus, the missing data may be predicted before reconstructing the image. Section II gives a brief review of the inverse scattering identity; more details can be found in [2]. In Section III, we define the sinogram. The sinogram recovery algorithm is described in Section IV. In Section V, we present experimental results that demonstrate the performance of the proposed method.

## II. Review of the Physical-Optics Inverse Scattering Identity

A rigorous time-domain inverse scattering identity has been derived in [2]. This uses both the physical optics (PO) induced currents and the "correction currents," which must be included to describe the non-PO effects. Since the correction terms are difficult to obtain under practical conditions, we will only consider the PO contributions in this paper.

Consider a perfectly conducting object illuminated by a transient plane wave. According to the PO approximation, the current induced on the object in the illuminated region will be simply

$$\vec{J}(\vec{r}, t) = 2\hat{n} \times \vec{h}^i(\vec{r}, t) \tag{1}$$

where $\vec{h}^i(\vec{r}, t)$ is the incident magnetic field, $\hat{n}$ is the unit vector normal to the scatterer surface, $\vec{r}$ is the position vector to the observation point, and $t$ denotes normalized time in

Manuscript received November 12, 1997; revised February 19, 1998.

The authors are with the Department of Electrical Engineering, Michigan State University, East Lansing, MI 48824 USA.

Publisher Item Identifier S 0018-926X(99)07962-4.

meters ($ct$). The far-zone field at a point $\vec{r}_s = r_s\hat{r}_s$ produced by this induced current is given by

$$\vec{h}^s(\vec{r}_s,t) = -\frac{1}{4\pi r_s}\int_s \hat{r}_s \times \frac{\partial \vec{J}(\vec{r}',\tau')}{\partial \tau'}\,ds' \tag{2}$$

where $\vec{r}'$ is the position vector to the integration point, $R_s = |\vec{r}_s - \vec{r}'|$, and $\tau' = t - R_s$. Substitution of (1) into (2) leads to the following relationship between incident and scattered fields:

$$\int_V \frac{\partial^2 h^i(\vec{r}',\tau)}{\partial \tau^2}\,dv' = \frac{\pi r_s}{(\vec{K}\cdot\hat{r})\cos(\beta/2)} H^s(\vec{r}_s,t) \tag{3}$$

Here, $h^i(\vec{r},t) = \hat{h}^i \cdot \vec{h}^i(\vec{r},t)$, $\vec{K} = \hat{r}_s - (\hat{r}_s\cdot\hat{h}^i)\hat{h}^i$, $R_i = |\vec{r} - \vec{r}_i|$ where $\vec{r}_i = r_i\hat{r}_i$ is the position vector of the transmitter, $\tau = t - R_i - R_s$, and $\hat{r}_i + \hat{r}_s = \hat{r}2\cos(\beta/2)$ where $\beta$ is the bistatic angle between the transmitter and the receiver. The total magnetic field is $H^s(\vec{r}_s,t) = \hat{h}^i \cdot [\vec{h}^s(\vec{r}_s,t) + \vec{h}^s_2(\vec{r}_s,t)]$, which is the sum of the scattered field and the scattered field under complimentary (shadow zone) illumination.

Now, consider the case of a band-limited incident field waveform. If $\vec{h}^i(\vec{r},t)$ has a time dependence given by the sine-modulated exponential pulse (SMEP) waveform

$$h^i(t) = \sin(\omega_c t)e^{-\alpha t}U(t) \tag{4}$$

then (3) can be written as

$$\begin{aligned}\int_{-\infty}^{\infty}\!\!\iint F(\vec{r}')\delta(t_s - \hat{r}\cdot\vec{r}')\,dv' &= \frac{2\pi r_s}{\vec{K}\cdot\hat{r}\omega_c}\Bigg[H^s(\vec{r}_s,t) + 2\alpha\int_0^t H^s(\vec{r}_s,t)\,dt \\ &\quad + (\omega_c^2+\alpha^2)\int_0^t\int_0^t H^s(\vec{r}_s,t)\,dt^2\Bigg]\end{aligned} \tag{5}$$

where $t_s = (r_i + r_s - t)/[2\cos(\beta/2)]$ and $F(\vec{r}')$ is the characteristic function of the scatterer defined over the volume $V$ of the scatterer as

$$F(\vec{r}') = \begin{cases} 1, & \vec{r}' \in V \\ 0, & \vec{r}' \notin V. \end{cases} \tag{6}$$

It is seen that the left-hand side of (6) is the cross-sectional area of the scatterer along the $\hat{r}$ direction. This is the Radon transform of $F(\vec{r}')$ and, thus, the characteristic function can be found by taking the three-dimensional inverse Radon transform. If the two-dimensional (2-D) inverse Radon transform is taken instead, the thickness function $f(x,y)$ for the target is obtained. Computing the transform in the $x$-$y$ plane gives (7), as shown at the bottom of the page, where $\vec{\rho}' = x'\hat{x} + y'\hat{y} = \rho'\cos\phi'\hat{x} + \rho'\sin\phi'\hat{y}$ and $\rho_{is} = \rho_i + \rho_s$. This 2-D, bistatic PO identity will be used to construct the images described in this paper.

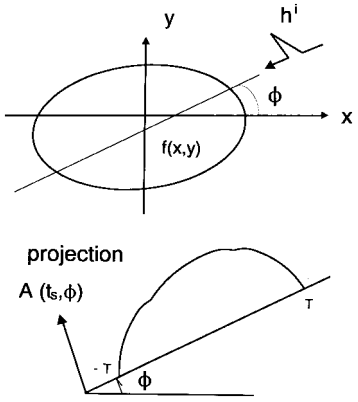


Fig. 1. The geometry of the 2-D Radon transform.

## III. Sinograms

Projection data (cross-sectional area functions) used for image reconstruction can be arranged in a 2-D map in which one of the coordinates is the distance of the wave along which the line integral is taken from the center of the rotation of the projection system and the other coordinate is the angle of the wave. In this map, waves through a fixed point in the object correspond to a sinusoidal curve, which is why a display of this map is called a sinogram [13].

Referring to the geometry of Fig. 1, we define the 2-D Radon transform by

$$A(\hat{r},t_s) = \int\int_{-\infty}^{\infty} f(x',y')\delta(t_s - (x'\cos\phi^i + y'\sin\phi^i))\cdot dx'\,dy' \tag{8}$$

where $f(x,y)$ is the 2-D "thickness function" of the object in the $z$ direction, and $A(\hat{r},t_s)$ is the projected area onto $t_s$ for the particular aspect angle $\phi$. In this paper, we assume $f(x,y)$ to be a real function defined on the disk of radius $T$ centered at the origin. A sinogram is an image of the 2-D Radon transform, where $t_s$ and $\phi$ form the horizontal and vertical axes, respectively, of a Cartesian coordinate system. Because of the periodicity of the 2-D Radon transform and because of the assumed domain of $f(x,y)$, the sinogram can be defined over the complete domain

$$\eta = \{(t_s,\phi)|t_s \in [-T,T], \phi \in [0,\pi]\}. \tag{9}$$

For the limited-view problem, the sinogram is measurable over a domain $\zeta$, where $\zeta$ is assumed to be a subset of $\eta$, i.e., $\zeta \in \eta$. Then $\zeta$ can be written as

$$\zeta = \{(t_s,\phi)|t_s \in [-T,T], \phi \in [\phi_L, \pi - \phi_L]\} \tag{10}$$

where $\phi_L$ is a constant that represents the data's missing angular range. In Fig. 2, we illustrate the measurement domains $\zeta$ given by (10).

$$f(\vec{\rho}) = -\frac{2\rho_s\cos(\beta/2)}{(\vec{K}\cdot\hat{\rho})\pi\omega_c}\int_0^{\pi}\int_{-\infty}^{\infty}\frac{H^s(\vec{\rho}_s',t) + 2\alpha\int_0^t H^s(\vec{\rho}_s',t)\,dt + (\omega_c^2+\alpha^2)\int_0^t\int_0^t H^s(\vec{\rho}_s',t)\,dt^2}{[t - \rho_{is} + 2\rho'\cos(\beta/2)\cos(\phi' - \phi^i + \beta/2)]^2}\,dt\,d\phi^i \tag{7}$$

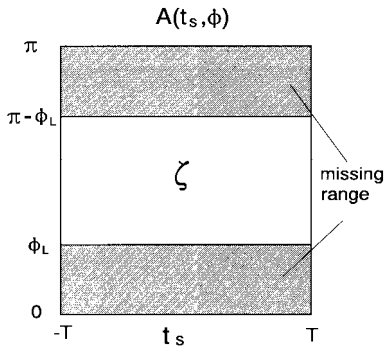


Fig. 2. Domain $\zeta$ over which the sinogram is measurable in the limited-view problem.

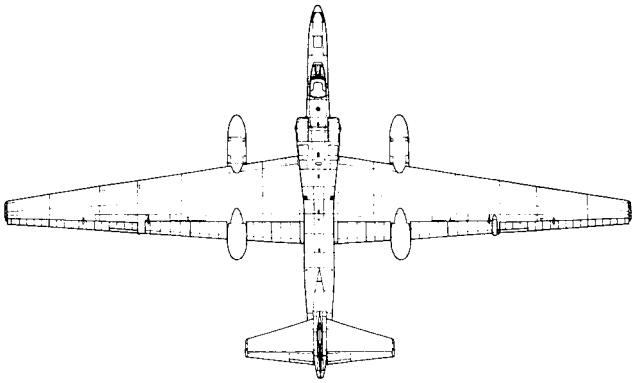

Fig. 3. A 1 : 48 scale model TR-1 aircraft.

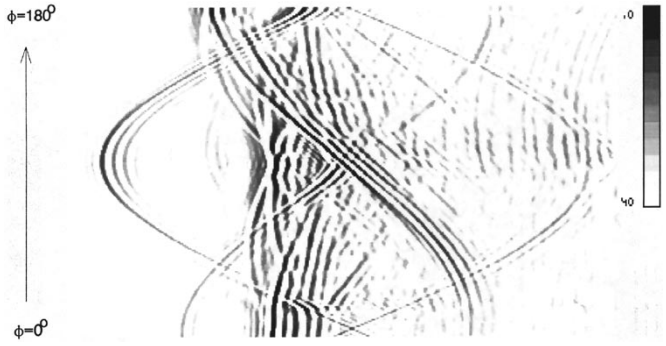


Fig. 4. Measured sinogram of TR-1 aircraft.

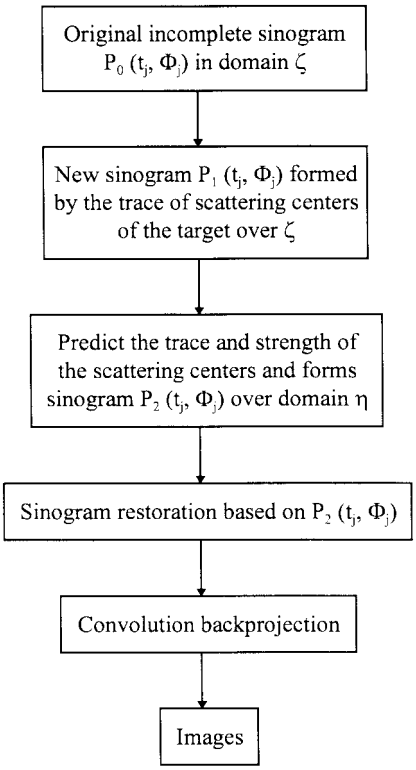


Fig. 5. Block diagram of the procedure needed to realize the reconstruction algorithm.

Figs. 3 and 4 show a 1 : 48 scale model TR-1 aircraft and its sinogram measured in the Electromagnetics Laboratory, Michigan State University. Note that the sinogram is formed not from the cross-sectional function, but from the SMEP responses of the target. We can see from the sinogram that most of the "lines" look sinusoidal. These lines are actually the traces of the scattering centers on the target. This motivates the idea of predicting the traces of the scattering centers using linear prediction. Linear prediction has been widely used in speech signal processing, image processing, and noise suppression in communication [14]. Here we use it in sinogram reconstruction in radar imaging for the limited-view problem. The following sections give a more detailed presentation of the approach.

## IV. The Algorithm

Fig. 5 shows the block diagram of the complete reconstruction algorithm used in this study. The projection data are expressed as $P(t,\phi)$ where $t$ and $\phi$ are the usual coordinates for the sinogram representation, i.e., $\phi$ is the angle of a projection line and $t$ is the coordinate perpendicular to the projection line. The algorithm starts from the original incomplete projection data $P_o(t_j,\phi_i)$ $(\phi_L \le \phi_i < \pi - \phi_L, 0 < \phi_L < \pi/2), i = 1, 2, \cdots, N_\phi, j = 1,2, \cdots, N_t$, where $N_\phi$ is the number of views and $N_t$ is the number of samples in each view. The first step is to isolate the largest specular reflections at each angle $\phi$ by isolating the major peaks embedded in each SMEP response. This can be difficult because of the temporal sidelobes of the SMEP waveform, but a smoothing window consisting of a Gaussian function of width slightly smaller than the SMEP duration can be used to smooth the responses. Then, the peak waveform values correspond to the positions of the scattering centers of the target. These peak values form a new sinogram from which the traces of the scattering centers can be found.

For each of the major scattering center traces, the temporal position and reflected amplitude are represented as a function of angle through the sampled pairs $(t_k,\phi_k)$ and $(P_k,\phi_k)$, $k = 1,2, \cdots, N_\phi$. The values over the missing angles are provided using a linear prediction algorithm. Letting $y_n$ represent either the sampled temporal position or reflected amplitude, the values of $y_n$ can be represented as a linear combination of its previous values and some input $x_n$ as

$$y_n = -\sum_{j=1}^{n} b_j y_{n-j} + x_n \tag{11}$$

where $N$ is a user-chosen parameter. Since $x_n$ represents the

discrepancy of the prediction at point $n$, we can determine the predictor coefficients $b_j$ through a least-squares minimization of the squared error

$$E = \sum_n e_n^2 = \sum_n \left( y_n + \sum_{j=1}^{N} b_j y_{n-j} \right)^2. \tag{12}$$

Setting the derivatives of the error with respect to the coefficients equal to zero gives the normal equations for the coefficients of the linear predictor

$$\gamma_y(k) = -\sum_{j=1}^{N} b_j \gamma_y(k-j) \qquad k = 1, 2, \cdots, N \tag{13}$$

where $\gamma_y(k) = \Sigma_n \, y_n y_{n-k}$. Noting that the minimum mean-square prediction error is simply

$$E_N = \gamma_y(0) + \sum_{j=1}^{N} b_j \gamma_y(-j) \tag{14}$$

an augmented set of normal equations can be obtained and written in matrix form as

$$\begin{bmatrix} \gamma_y(0) & \gamma_y(1) & \cdots & \gamma_y(N-1) \\ \gamma_y(1) & \gamma_y(0) & \cdots & \gamma_y(N-2) \\ \vdots & \vdots & \vdots & \\ \gamma_y(N-1) & \gamma_y(N-2) & \cdots & \gamma_y(0) \end{bmatrix} \begin{bmatrix} 1 \\ b_1 \\ \vdots \\ b_N \end{bmatrix} = \begin{bmatrix} E_N \\ 0 \\ \vdots \\ 0 \end{bmatrix}. \tag{15}$$

This matrix is of the symmetric Toeplitz type and many efficient algorithms are available for solving this set of linear equations [14]. In this work, we used the Levinson–Durbin algorithm.

To ensure stability of the linear prediction of the coefficients $b_j$, the roots of the characteristic polynomial

$$z^N - \sum_{j=1}^{N} b_j z^{N-j} = 0 \tag{16}$$

are computed. If any roots are outside the unit circle, they are moved to an appropriate point inside or on the unit circle and the coefficients $b_j$ are recalculated. In addition, the value of $N$ should be chosen as small as practicable; we used between 5 and 15, depending on the data length.

Once the coefficients $b_j$ are determined, the scattering center traces are reconstructed over the domain $\eta$. Then, for each view angle over the missing region, the scattering center positions are predicted. A narrow window of rectangular shape is placed around each scattering point and the window is multiplied by a SMEP defined in (5) and, thus, the predicted SMEP response is found for this view. After predicting all the SMEP responses over the missing data region in domain $\eta$, we can restore the complete sinogram over the domain $\eta$. Finally, the image is constructed by using the convolution backprojection method with the restored sinogram [2].

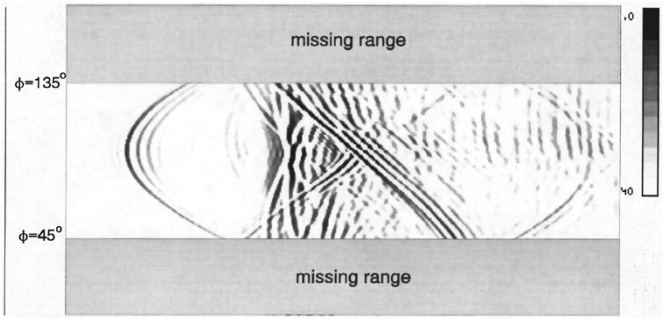


Fig. 6. Measurable part of the sinogram of TR-1 aircraft.

We can see that accurate reconstruction of the sinogram depends on several variables. A wider range of views will obviously allow a more accurate prediction of the missing data, but it is very difficult to quantify the relationship between available range and quality of reconstructed image. If the available range includes regions where the scattering center responses are strong, and sufficient variation in the magnitude and position is included, then the reconstruction will be correspondingly accurate. If, on the other hand, a scattering center is shadowed throughout the available range, then there will be no way that the scattering center trace can be predicted in the missing data region. In the simulation to follow, we use a range of 90° and are able to very accurately predict the traces of the five most significant scattering centers. The number of scattering centers traced also influences the quality of the final image. Using more scattering centers allows the reconstruction of smaller target structures, but the traces of weaker scattering centers are hard to discern and confusion between scattering centers leads to anomalous image features.

## V. Imaging Simulation

The proposed algorithm in Section IV can be used in the time domain to construct an image from limited-view ultrawide-band radar measurements. Consider the sinogram of the TR-1 aircraft model shown in Fig. 4. When only part of the sinogram (domain $\zeta$) as shown in Fig. 6 is measurable, then the reconstructed image may be seriously distorted if we simply let the missing data be zero. To restore the complete sinogram (domain $\eta$) using linear prediction techniques before reconstructing the image by the convolution backprojection algorithm, we first find the largest points (the darkest points in Fig. 6) in each SMEP response by comparing the values of the data in each view. Those points with large amplitude form a new sinogram. Fig. 7 shows the measurable sinogram of the TR-1 formed by these points, while Fig. 8 gives the complete sinogram of the TR-1 formed by these points assuming all views are measurable. From the new sinogram of Fig. 7, we can find the traces of the scattering centers and obtain a set of functions, each function designating the movement of a scattering center with the change of view. In Fig. 8, for example, numbers 3 and 4 denote the movements of the tail

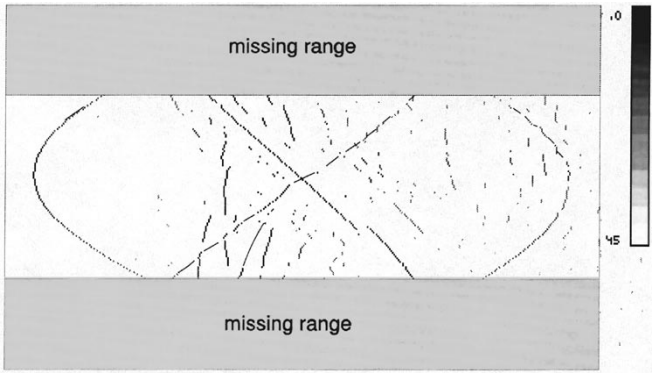


Fig. 7. Measurable part of the sinogram of TR-1 formed by the positions of the scattering centers.

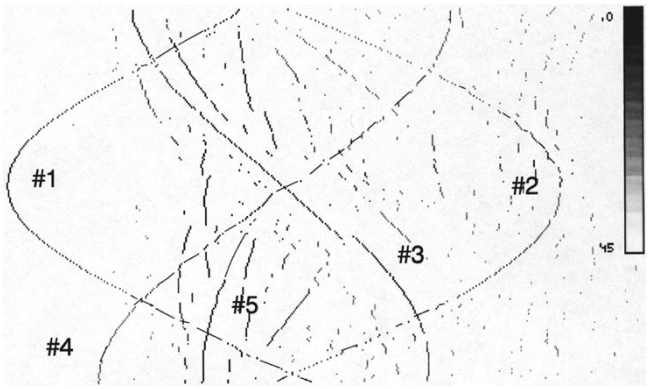


Fig. 8. Sinogram of TR-1 formed by the positions of the scattering centers.

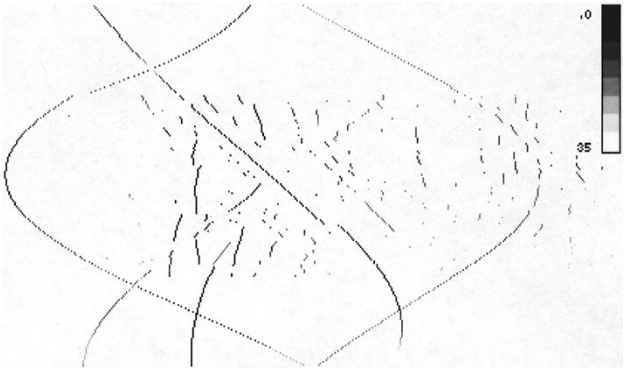

Fig. 9. Sinogram of TR-1 formed by the predicted positions of the scattering centers.

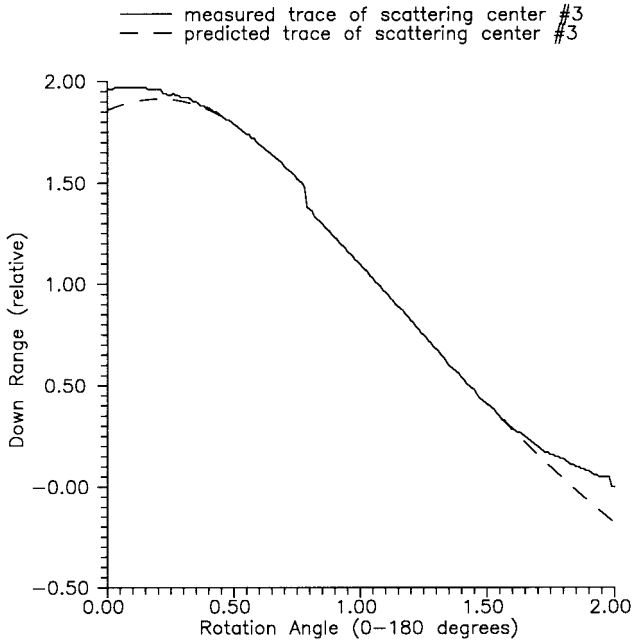


Fig. 10. Measured and predicted positions of the tail of the TR-1 aircraft.

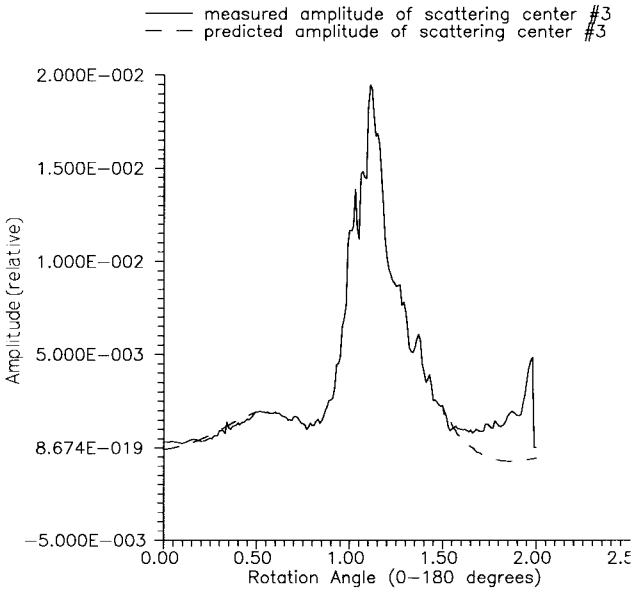


Fig. 11. Measured and predicted amplitude of the scattered field in the positions of the tail of the TR-1.

and the head of the aircraft model, respectively; numbers 1 and 2 denote the movements of two wings; and number 5 denotes the movement of the engines. Next, the movement and strength of the scattering centers is predicted over the whole sinogram region $\eta$ using linear prediction techniques. Fig. 9 shows the predicted traces of the scattering centers. Fig. 10 gives the trace of the tail with measured and predicted data and Fig. 11 gives the measured and predicted amplitudes of the scattered field at the positions of the tail.

We are now ready to reconstruct the sinogram of the target over the domain $\eta$ by finding those predicted scattering centers for each view over the missing region, placing a small rectangular window around each scattering point and multiplying the window by a SMEP defined in (4). Then the predicted SMEP responses are found for this view. Fig. 12 shows the measured data and the predicted data for observation angle $\phi = 40.5°$. The restored complete sinogram is shown in Fig. 13 after predicting all the SMEP responses over the missing data region in the domain $\eta$. Finally, we can reconstruct the image using the convolution backprojection method [2] with the restored sinogram. Fig. 14 gives the image of the TR-1 aircraft model using the restored sinogram and Fig. 15 gives the image of the TR-1 using the original incomplete sinogram shown in Fig. 6. We can see significant improvement in the quality of the reconstructed images from using the sinogram restoration techniques.

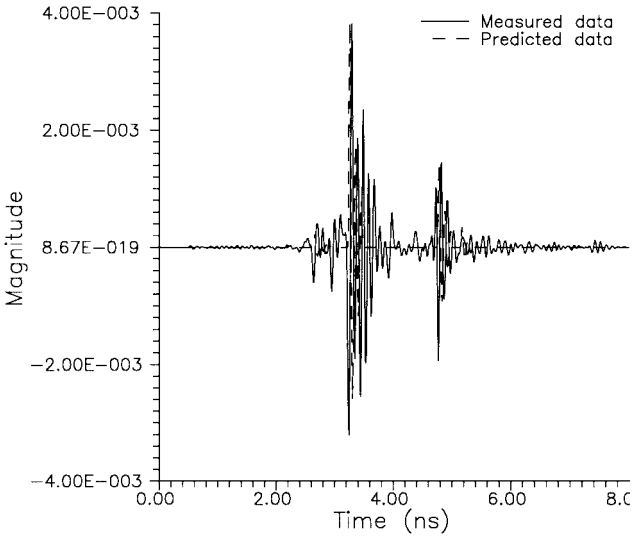


Fig. 12. Measured and predicted data of the TR-1 for $\phi = 40.5°$.

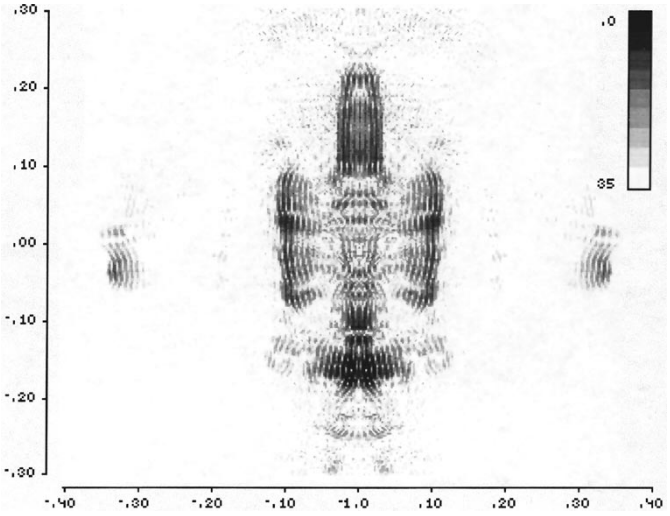

Fig. 15. Image of the TR-1 from 45° to 135° data using convolution backprojection algorithm.

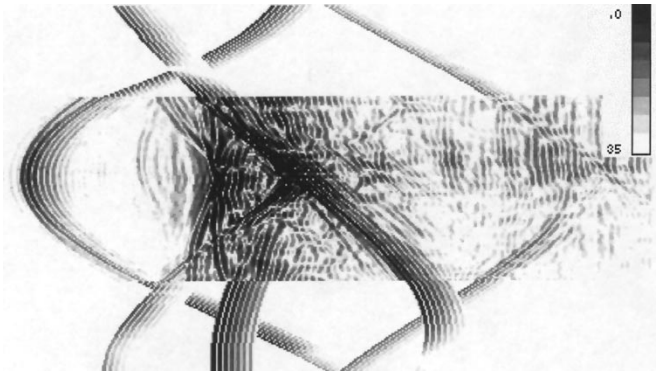

Fig. 13. Restored sinogram of the TR-1 by linear prediction method.

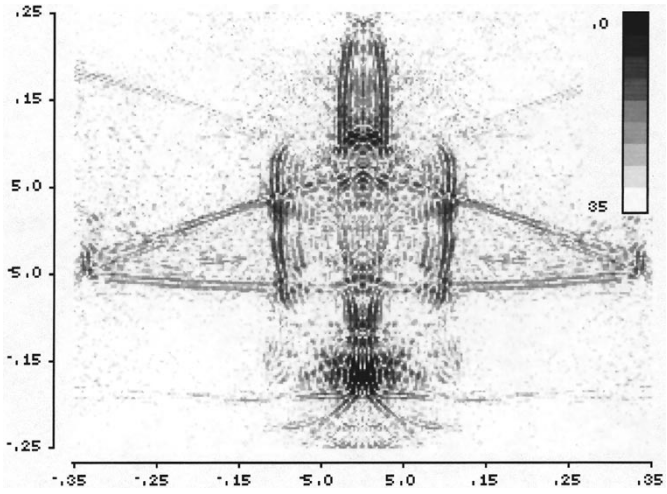

Fig. 14. Image of the TR-1 using restored sinogram.

## VI. Conclusions

We have proposed a technique to handle the time-domain limited-view imaging problem. The key point of this technique is to process the available measured projections in order to generate an estimate of the full set of projections, an image of which is called a sinogram. The goal of this approach is to recover the sinogram from the available measured data using linear prediction. Since the scattered field of a target can be written as a superposition of distinct specular reflections arising from scattering centers on the target, the position and strength of the scattering centers can be predicted using linear prediction with the change of the observation angle. Thus, the missing data can be predicted before reconstructing the image. A significant improvement in image reconstruction has been achieved using this technique, and some useful results have been provided.

## References

[1] Y. Dai, E. J. Rothwell, D. P. Nyquist, and K. M. Chen, "Time-domain imaging of radar targets using ultra-wideband or short pulse radars," in *IEEE AP-S Int. Symp. URSI Radio Sci. Meet.*, Newport Beach, CA, June 1995, p. 267.

[2] Y. Dai, E. J. Rothwell, K. M. Chen, and D. P. Nyquist, "Time-domain imaging of radar targets using algorithms for reconstruction from projections," *IEEE Trans. Antennas Propagat.*, vol. 45, pp. 1227–1235, Aug. 1997.

[3] A. K. Louis, "Picture reconstruction from projections in restricted range," *Math. Methods Appl. Sci.*, vol. 2, pp. 209–220, 1980.

[4] T. Inoye, "Image reconstruction with limited angle projection data," *IEEE Trans. Nucl. Sci.*, vol. NS-26, pp. 2666–2669, 1979.

[5] J. A. Reeds and L. A. Shepp, "Limited angle reconstruction in tomography via squashing," *IEEE Trans. Med. Imag.*, vol. MI-6, pp. 89–97, 1987.

[6] M. I. Sezan and H. Stark, "Tomographic image reconstruction from incomplete view data by convex projections and direct Fourier inversion," *IEEE Trans. Med. Imag.*, vol. MI-3, pp. 91–98, June 1984.

[7] L. M. Bregman, "Finding the common point of convex sets by the method of successive projections," *Doki. Akad. Nauk USSR*, vol. 162, no. 3, pp. 487–490, 1965.

[8] L. G. Gubin, B. T. Polyak, and E. V. Raik, "The method of projections for finding the common point of convex sets," *USSR Comput. Math. Phys.*, vol. 7, no. 6, pp. 1–24, 1967.

[9] D. C. Youla and H. Webb, "Image reconstruction by the method of projections onto convex sets-Part I," *IEEE Trans. Med. Imag.*, vol. MI-1, pp. 81–94, Oct. 1982.

[10] K. M. Hanson G. W. Wecksung, "Bayesian approach to limited-angle reconstruction in computed tomography," *Appl. Opt.*, vol. 24, pp. 4028–4039, Dec. 1980.

[11] P. Oskoui-Fard and H. Stark, "Tomographic image reconstruction using the theory of convex projections," *IEEE Trans. Med. Imag.*, vol. 7, pp. 45–58, Mar. 1988.

[12] J. L. Prince and A. S. Willsky, "Hierarchical reconstruction using geometry and sinogram restoration," *IEEE Trans. Image Processing*, vol. 2, pp. 401–416, July 1993.
[13] G. T. Herman, *Image Reconstruction from Projections: The Fundamentals of Computerized Tomography*. New York: Acdemic, 1980.
[14] J. G. Proakis and D. G. Manolakis, *Digital Signal Processing, Principle, Algorithm, and Applications*. New York: Macmillan, 1992.

**Yingcheng Dai** was born in Hubei, China. He received the B.S. and M.S. degrees in electrical engineering from University of Electronic Science and Technology, Chengdu, China, in 1988 and 1991, respectively, and the Ph.D. degree in electrical engineering from Michigan State University, East Lansing, Michigan, in 1997.

In 1998, he joined Harada Industry of America, Novi, Michigan, where he is engaged in the research and development of FM/AM, GPS, TV, and digital cellular antennas for automotive applications.

**E. J. Rothwell** (S'84–M'85–SM'92), for a photograph and biography, see p. 1278 of the September 1998 issue of this TRANSACTIONS.

**K. M. Chen** (SM'64–F'76), for a photograph and biography, see p. 1278 of the September 1998 issue of this TRANSACTIONS.

**D. P. Nyquist** (S'63–M'67–SM'92–F'97), for a photograph and biography, see p. 1278 of the September 1998 issue of this TRANSACTIONS.